

OBSERVATION OF QUASI-PERIODIC COMPRESSIVE WAVES IN SOLAR POLAR PLUMES

C. E. DEFOREST¹ AND J. B. GURMAN

NASA/Goddard Space Flight Center, *SOHO* Experimenters' Analysis Facility, Code 682.3, Building 26, Room G-1, Greenbelt, MD 20771;
cdeforest@solar.stanford.edu, jgurman@solar.stanford.edu

Received 1997 October 23; accepted 1998 March 31; published 1998 June 26

ABSTRACT

On 1996 March 7, the *Solar and Heliospheric Observatory* spacecraft conducted a multi-instrument campaign to observe polar plumes in the south polar coronal hole. Recent time-domain analyses of EUV Imaging Telescope images from that campaign show filamentary substructure in the plumes, on a length scale of $\sim 5''$, which changes on timescales of a few minutes, and coherent quasi-periodic perturbations in the brightness of Fe IX and Fe X line emission at 171 \AA from the plumes. The perturbations amount to 10%–20% of the plumes' overall intensity and propagate outward at $75\text{--}150 \text{ km s}^{-1}$, taking the form of wave trains with periods of 10–15 minutes and envelopes of several cycles. We conclude that the perturbations are compressive waves (such as sound waves or slow-mode magnetosonic waves) propagating along the plumes. Assuming that the waves are sonic yields a mechanical energy flux of $150\text{--}400 \text{ W m}^{-2}$ ($1.5\text{--}4 \times 10^5 \text{ ergs cm}^{-2} \text{ s}^{-1}$) in the plumes.

Subject headings: Sun: corona — Sun: solar wind — Sun: UV radiation

1. INTRODUCTION

Polar plumes are cool, dense, linear, magnetically open structures that arise from predominantly unipolar magnetic footpoints in the solar polar coronal holes, subtending roughly 2° relative to Sun center at low altitude and expanding super-radially with the coronal hole (Newkirk & Harvey 1968; DeForest et al. 1997). With topologically simple structure and little impulsive activity, they are among the more quiescent features in the lower solar corona. Because of the relative simplicity of polar plumes, learning about their heating and acceleration mechanisms is important to understanding the “background” processes that heat the entire corona.

The EUV Imaging Telescope (EIT) (Delaboudinière et al. 1995), with its relatively high exposure rate, signal-to-noise ratio, and resolution, provides a new window into plume behavior on timescales of a few minutes and spatial scales of a few arcseconds. Previous plume models have generally assumed a uniform cross section for each plume and have neglected time dependence (e.g., Habbal 1992; Walker et al. 1993; Wang 1994). Karovska et al. (1994) claim to have seen filamentary structure in polar plumes with *Skylab* data, and work by Withbroe (1983) has provided evidence that plumes fluctuate in brightness by $\sim 10\%$ on timescales of a few minutes. The high quality of the EIT data allows considerable advances in both of these areas. In the present Letter, we demonstrate that there is filamentary structure within plumes on a spatial scale of $3''\text{--}5''$, which changes on a timescale of a few to 10 minutes, and that there are coherent outwardly propagating brightness structures that propagate at $\sim 75\text{--}150 \text{ km s}^{-1}$ and recur quasi-periodically on timescales of ~ 10 minutes.

2. OBSERVATIONS

On 1996 March 7, the *Solar and Heliospheric Observatory* (*SOHO*) (Fleck et al. 1995) engaged in a campaign to search for and characterize signs of wave activity in polar plumes. A full description of the observations has been published (DeForest et al. 1997). The observations included an EIT sequence of 104 frames, spaced at less than 3 minute intervals, of the

south polar coronal hole in the 171 \AA (Fe IX and Fe X) passband. The exposure time was 7 s.

A single EIT frame from that observation, with a radial background model corona subtracted (§ 3.2 below), is shown in Figure 1. Several bright plumes were observed during the minicampaign, typically extending from the base of the corona to $\sim 1.3 R_\odot$ before fading into the background noise. The plumes remained relatively constant in overall 171 \AA brightness for periods of up to several hours. However, movies made from the sequence were observed to have a wavering, “ripply” appearance, which hints that small-scale motions might be occurring. Six of the brightest plumes and one nonplume region, all marked in Figure 1, were selected for analysis.

Figure 2 shows plume 2 (there is another plume visible in the background) as seen in several frames of the sequence. The pictured frames are separated by 9 minutes (i.e., three frames) and have been background-subtracted to increase contrast. Each of the two pictured plumes shows distinct filamentary structures within its core. The filamentary structures change their overall shape dramatically during the 9 minutes between each of the images in Figure 2.

3. ANALYSIS

Preliminary analysis of the raw EIT data proceeded in four independent steps: exposure normalization, background subtraction, three-dimensional feature tracking, and evolution chart synthesis.

3.1. Exposure Normalization

The raw images downlinked from EIT showed global brightenings and dimmings that are not solar in origin; they are caused by small ($\sim 5\%$) random variations in the frames' exposure time. Because the EIT detector response is linear in total exposure (Delaboudinière et al. 1995), a linear scaling of each image's pixels can correct for the offsets. We divided each frame by the total observed fluence in that frame to remove the global brightness variations induced by the variations in exposure time. This step assumes that the actual total Fe IX/Fe X luminosity of the coronal hole does not change much from frame to frame; this *Ansatz* is justified by the sub-

¹ C. E. D. is employed by Stanford University, on location at NASA/GSFC.

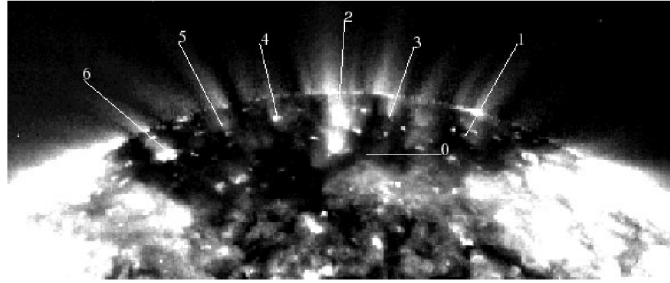


FIG. 1.—Polar plumes over the south pole of the Sun as seen in the EIT 171 Å (Fe IX/Fe X) passband. A radial background model of the corona has been subtracted from this image. Several plume regions used in the text are labeled. Note that region 0 is a “null region” used as a control case.

sequent lack of global variations in the brightness of randomly chosen, moderate-sized features in the images (see § 3.4).

3.2. Background Subtraction

In order to increase contrast, a radial background model corona was generated for the data set and subtracted from each image. The background coronal image was generated by finding the lowest valued pixel in the entire data set for each radius from disk center (binned into 1 pixel bins), then smoothing over 10 bins in the radial array of minimum values. This array of minimum pixel values was taken to represent the brightness of a spherically symmetric background corona. Values from the array were then subtracted from each scaled raw image to obtain background-subtracted coronal images such as Figure 1. The limb of the Sun is still slightly visible in the background-subtracted images because of the 10 bin smoothing of the radial model.

3.3. Feature Tracking

To look for moving features in the plumes, it was necessary to remove the effects of solar rotation. Because the plumes rotate with the Sun in three dimensions, it was necessary to apply a geometric model to track each plume’s motion in the image plane. We treated each plume as a linear feature that is coplanar with the meridian on which it rested and that is rotating

rigidly with the solar rotation speed at its footpoint. This geometrical model was used to position each image so as to center the plume in a small subfield, oriented vertically (as in the images of plume 2 in Fig. 2). In each case, this a priori geometry was found to work well enough to keep the plume centered to within a small fraction of its cross-sectional width.

3.4. Evolution Chart Synthesis

To identify coherent motions along the plumes, we generated synoptic-like maps of the evolution of each plume’s core using the derotated sequences of subfields. We extracted a vertical strip of the middle few pixels of each image and laid the strips side by side to produce a time evolution chart of the plume’s brightness. Figure 3 is such an evolution chart for plume 1. The main visible features are the limb of the Sun and the bottom of the plume (with a bright point just under it). The timing between original exposure frames was variable (between 1 and 3 minutes), so the spacing (and size) of the image strips is variable as well to keep the time axis accurate.

Finally, to emphasize only the time-variable aspects of the plumes’ behavior, we subjected each evolution chart to a running-difference process: each frame had the subfield from 6 minutes prior subtracted from it. In cases in which there was no image taken exactly 6 minutes prior, the subtracted image was linearly interpolated from the surrounding frames. The top panel of Figure 4 is such a running-difference strip chart for plume 1.

If the effective exposure time varied between images in this data set, then individual frames would appear brighter or darker than their companions—which would appear on this chart as vertical striations. The lack of vertical striations (other than the edges of the strips themselves) justifies the *Ansatz* in § 3.1 above.

4. RESULTS

In the differenced charts, there are clear diagonal features not easily seen in Figure 3. The bright diagonal ridges represent traveling regions of slightly higher and lower brightness in the plume. One may read off the propagation speed of a feature merely by measuring its slope on the chart.

Outward-propagating features are visible in every plume evolution chart that we made. Plume 1 and plume 5 are shown in Figure 4. Plume 1 shows propagation speeds of ~ 110 km s^{-1} throughout. Plume 5 exhibits two distinct propagation speeds: 80 ± 10 km s^{-1} (*right*) and 140 ± 20 km s^{-1} (*left*). The slowest features that we saw propagated at 75 ± 10 km s^{-1} and were in plume 2; the fastest are the ones visible in plume 5. There is no discernible acceleration or deceleration

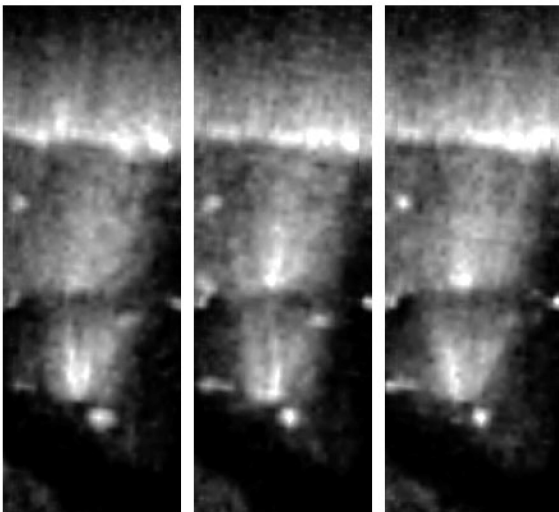


FIG. 2.—Four views of plume 2, taken 9 minutes apart (two plumes are visible). Note the large changes in brightness and overall structure of each plume between adjacent frames.

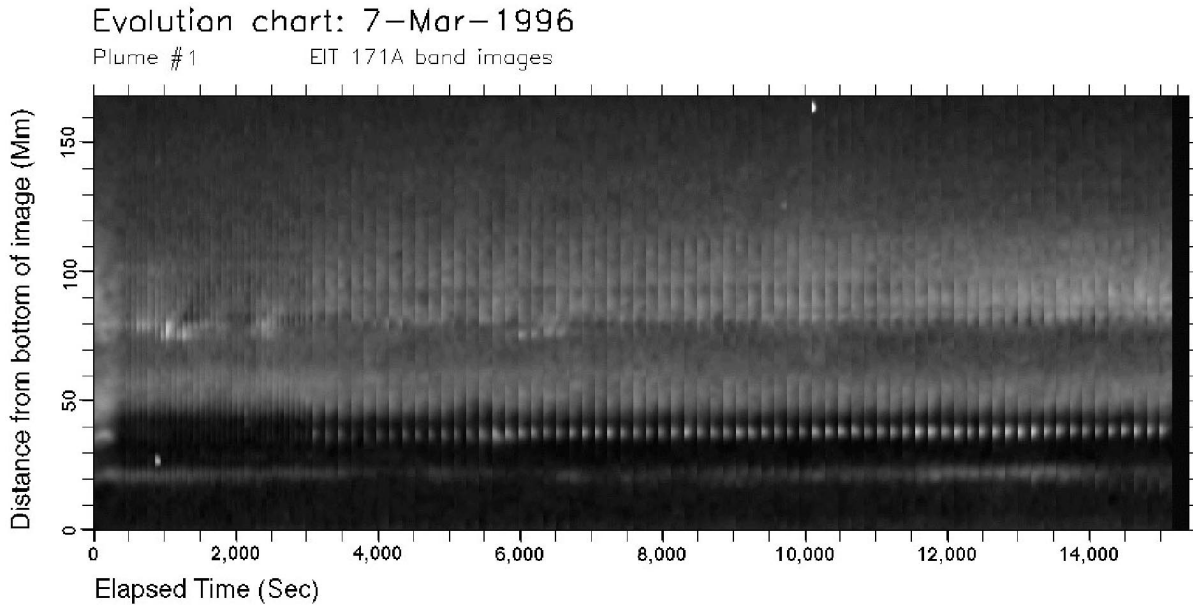


FIG. 3.—Evolution chart for plume 1, which is different than the plume shown in Fig. 2. The large horizontal bands represent the foot of the plume and the limb of the Sun. The bright horizontal line below the plume is a coronal bright point.

of any individual feature as it propagates (with the observed signal-to-noise ratio, though, the features could change speed by as much as 20% from base to top without detection).

The ridges in the evolution chart brightness are not isolated; they appear in groups of ~ 3 – 10 at intervals of 600 – 900 s. They are quasi-periodic: even within a particular group of ridges, there is no single cadence on which the ridges regularly recur. The duty cycle is roughly balanced: neither the crests nor the troughs of brightness are especially short compared to the other.

The variations amount to a 10%–20% variation in the background-subtracted brightness of each plume in 171 \AA light, which corresponds to a 5%–10% change in electron density (provided that there are no associated temperature effects that are large enough to bring the plasma out of the telescope's band of sensitivity).

5. DISCUSSION

Sheeley et al. (1997) have identified moving low-latitude structures in the large-angle spectrometric coronagraph (LASCO) C-2 images as tracers of the slow solar wind. Similarly, they have identified some transient, traveling features that may be tracers of the fast solar wind over the coronal holes. The present moving features visible in polar plumes in EIT are different in three important respects: (1) they move at a constant speed throughout our field of view, while Sheeley's tracers accelerate as they move out; (2) they are repeated in quasi-periodic trains, while Sheeley's tracers are isolated; and (3) they are present in every plume that we have studied, while the tracers are only present occasionally. Finally, spectroscopic measurements of similar plumes do not show Doppler blue-shifts corresponding to bulk motion at the observed speeds (Hassler et al. 1998), which indicates that the fluctuations do not correspond to bulk flows.

Because of these four key points, we identify the observed features as compressive waves rather than outflowing features. Because they are traveling at or under the calculated sound speed in the plumes, we consider them to represent sonic or slow magnetosonic modes.

Assuming that the propagating features are waves, we estimated their mechanical energy flux. We considered the features to be sinusoidal sound waves with an amplitude of 5%, propagating through a typical plume plasma (DeForest 1995; Ahmad & Withbroe 1977; Walker et al. 1993) of temperature $1 \times 10^6 \text{ K}$ and electron density 10^9 cm^{-3} . Using $v_s = 75 \text{ km s}^{-1}$, $\gamma = 5/3$, and $n = n_i + n_e = 2n_e$ yields a sonic energy flux of 150 W m^{-2} , or $1.5 \times 10^5 \text{ ergs cm}^{-2} \text{ s}^{-1}$. This is a lower bound because we have used the lower bounds for measured wave amplitude and speed and have assumed the wave mode with the lowest energy per unit amplitude (despite the fact that the calculated sound speed is $\sim 150 \text{ km s}^{-1}$ for these conditions, which is close to the highest speed that we detected). Using the higher values of 150 km s^{-1} for the sound speed and 10% for the density amplitude yields an upper-bound energy flux of 600 W m^{-2} ; but the maximum measured amplitude and speed did not occur simultaneously. The highest energy flux that we actually measured by this method is in plume 5, at $\sim 400 \text{ W m}^{-2}$ for the waves propagating at 140 km s^{-1} .

6. CONCLUSIONS

We have observed compressive waves traveling through polar plumes in the 10–15 minute frequency range and have identified them as sonic or slow-mode magnetosonic waves. The fluctuations are quasi-periodic compressive wave trains. Their amplitude is about 5%–10% in density, and the waves travel at a roughly constant speed throughout the altitude range 1.01 – $1.2 R_\odot$, carrying an estimated mechanical energy flux of 150 – 400 W m^{-2} . We cannot, with the present measurement, distinguish between sound waves and other modes which may carry additional magnetic energy; however, the quoted range is a lower bound for the entrained energy regardless of mode.

The presence of high-amplitude waves is significant to coronal hole heating and wind acceleration models, which require input of both momentum and energy. Our observed energy flux, which is a few hundred watts per square meter (a few times $10^5 \text{ ergs cm}^{-2} \text{ s}^{-1}$), is comparable to the energy flux required to heat the coronal hole, which is about 1 kW m^{-2}

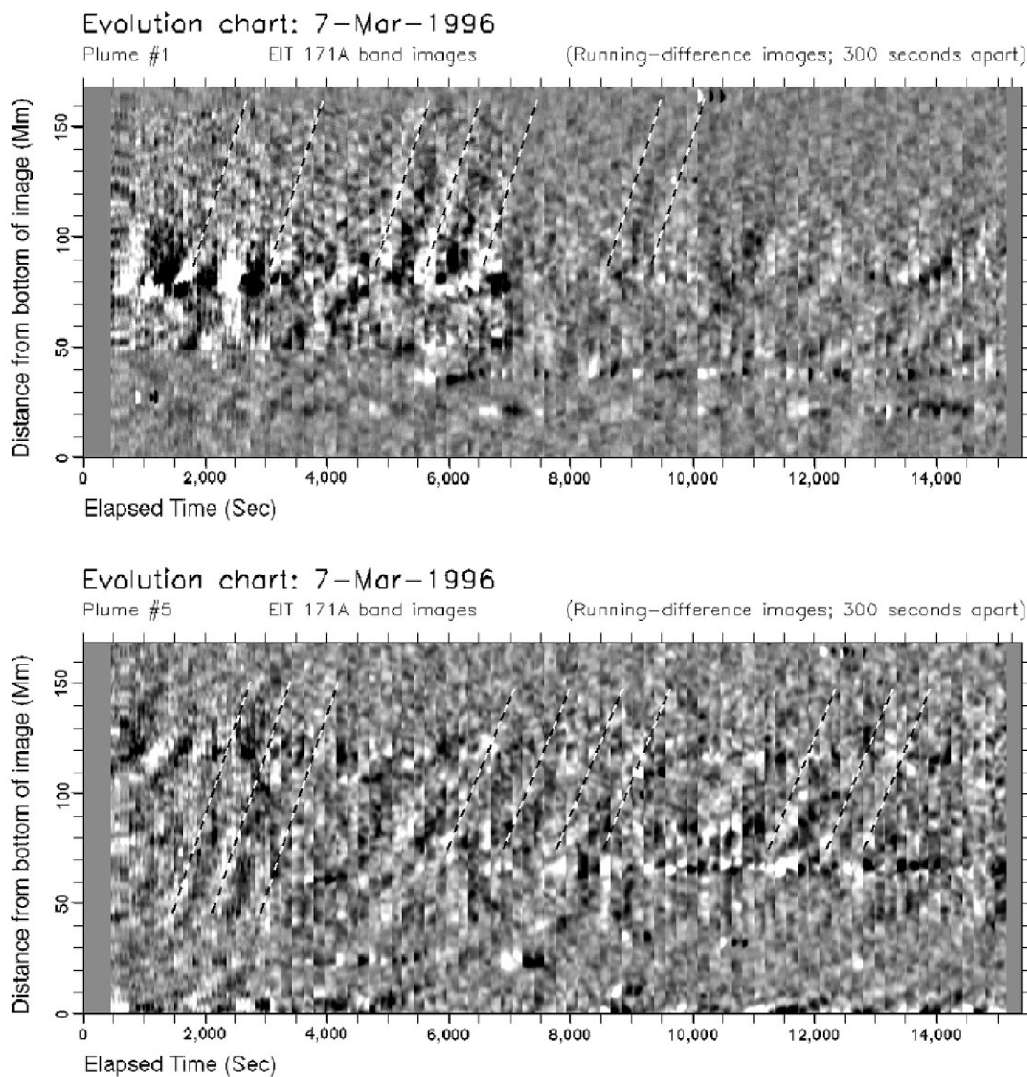


FIG. 4.—Differenced evolution charts for plumes 1 and 5. Each vertical strip (from Fig. 3) has been replaced by its difference from the strip 360 s previous to it. The contrast has been greatly increased. Diagonal (moving) features are readily apparent; several have been marked. The features in the top panel are traveling at $\sim 100 \text{ km s}^{-1}$; those in the bottom panel are traveling at ~ 140 (left) and $\sim 80 \text{ km s}^{-1}$ (right).

($10^6 \text{ ergs cm}^{-2} \text{ s}^{-1}$; Parker 1991). Future studies will characterize the observed waves more thoroughly and attempt to model their propagation through and effect on the plume plasma.

Thanks are due Leon Ofman, Yi-Ming Wang, and Neil Shee-

ley for several insightful discussions and to the referee for helping make this article more complete and readable. C. E. D. is supported by NASA grant NAG5-3077. *SOHO* is a project of international collaboration between NASA and ESA.

REFERENCES

- Ahmad, I. A., & Withbroe, G. L. 1997, *Sol. Phys.*, 53, 397
 DeForest, C. E. 1995, Ph.D. thesis, Stanford Univ.
 DeForest, C. E., et al. 1997, *Sol. Phys.*, 175, 393
 Delaboudinière J.-P., et al. 1995, *Sol. Phys.*, 162, 291
 Fleck, B., Domingo, V. L., & Poland, A. I., eds. 1995, *The SOHO Mission* (Dordrecht: Kluwer)
 Habbal, S. R. 1992, *Ann. Geophys.*, 10, 34
 Hassler, D. M., Wilhelm, K., Lemaire, P., & Schuehle, U. 1998, *Sol. Phys.*, in press
 Karovska, M., et al. 1994, *ApJ*, 428, 854
 Newkirk, G., Jr., & Harvey, J. 1968, *Sol. Phys.*, 3, 321
 Parker, E. N. 1991, *ApJ*, 372, 719
 Sheeley, N. R., et al. 1997, *ApJ*, 484, 472
 Walker, A. B. C., DeForest, C. E., Hoover, R. B., & Barbee, T. D. W. 1993, *Sol. Phys.*, 148, 239
 Wang, Y.-M. 1994, *ApJ*, 435, L153
 Withbroe, G. L. 1983, *Sol. Phys.*, 89, 77